# Towards More Accurate Iris Recognition using Cross-Spectral Matching

N. Pattabhi Ramaiah, Ajay Kumar

***Abstract*—Iris recognition systems are increasingly deployed for large-scale applications such as national ID programs which continue to acquire millions of iris images to establish identity among billions. However with the availability of variety of iris sensors that are deployed for the iris imaging under different illumination/environment, significant performance degradation is expected while matching such iris images acquired under two different domains (either sensor-specific or wavelength-specific). This paper develops a domain adaptation framework to address this problem and introduces a new algorithm using Markov random fields (MRF) model to significantly improve cross-domain iris recognition. The proposed domain adaptation framework based on the naive Bayes nearest neighbor classification uses a real-valued feature representation which is capable of learning domain knowledge. Our approach to estimate corresponding visible iris patterns from the synthesis of iris patches in the near infrared iris images achieves outperforming results for the cross-spectral iris recognition. In this paper, a new class of bi-spectral iris recognition system that can simultaneously acquire visible and near infra-red images with pixel-to-pixel correspondences is proposed and evaluated. This paper presents experimental results from three publicly available databases; PolyU cross-spectral iris image database, IIITD CLI and UND database, and achieve outperforming results for the cross-sensor and cross-spectral iris matching.**

***Index Terms*—Biometrics, Iris recognition, Cross-Spectral, iris recognition, Cross-Sensor iris recognition, Domain adaptation.**

## I. Introduction

IRIS recognition [1], [2] plays an important role in uniquely identifying a person and is based on the uniqueness of iris texture. As compared to several other biometrics, iris recognition system is believed to be more reliable, accurate and scalable for person identification. Therefore the iris recognition system is widely used in large-scale national ID programs (e.g., Indias Aadhaar program) for processing over millions/billions of peoples biometric data. However several challenges emerge when the iris images acquired in one domain (sensor or illumination) is matched against the images acquired in different domain. Such cross-domain iris recognition problem includes the cases when the images in one domain represent the sensor-specific iris images or wavelength-specific iris images. This cross-domain iris recognition problem is briefly discussed in two different contexts of iris cross-comparisons.

The first context is the development of advanced cross-spectral iris recognition capability. Commonly deployed iris recognition systems [1], [3] use the iris images acquired from close distances under near infra-red (NIR) wavelengths. There have been several efforts [4], [5] to develop visible wavelength based iris recognition capabilities in order to eliminate the limitations of the iris recognition systems that require close range iris imaging under near-infrared illumination which can be hazardous. The surveillance data is often acquired under visible wavelengths. Therefore the applications like automated watch-list identification and surveillance at-a-distance requires accurate iris matching capability for images acquired under different wavelengths. In this context, simultaneously acquired visible iris images should be matched with the iris images acquired under near infra-red illumination to ascertain cross-spectral iris recognition accuracy. The experimental observations presented in section VII-C for such the cross-spectral iris matching problem also illustrate serious degradation in matching accuracy.

The other context of cross-domain iris recognition problem is cross-sensor iris matching problem which requires the data acquired from two different iris sensors to be accurately matched. The large-scale national ID programs are known to offer flexibility (reduce vendor dependence) and permits the use of iris sensors from multiple vendors in order to reduce the re-enrollment costs and time. The Aadhaar program certifies 15 different vendors for supplying the iris readers that meet quality specifications from STQC (Standardization Testing and Quality Certification) directorate [6]. The performance degradation when the iris image data acquired from the one sensor is matched with the iris image data acquired from the different iris sensor is scientifically known and can be attributed to the variations in sensor sensitivity, optics or the employed near infrared illumination.

In this paper, we develop and investigate two approaches to address the cross-domain iris recognition problem. In the first approach, we propose a classification framework based on NBNN domain adaptation in order to improve the matching performance for cross-domain (cross-spectral/cross-sensor) iris recognition systems. The Naive-Bayes Nearest-Neighbor (NBNN) [7], [8], [9] classifier uses the image-to-class (I2C) distance learning. Almost all the domain adaptation algorithms available today use I2I learning while I2C has only been attempted in NBNN framework for domain adaptation (DA-NBNN) [10]. This approach has not yet received attention in biometrics and has also been explored in this paper for the challenging problems in iris recognition.

This framework is further investigated and extended to improve the cross-domain iris matching capability by adopting the idea of spatial pyramid matching (SPM) [11]. The SPM based approach adopted in this paper can consider local iris pixel information at various level and generate localized pixel similarity measure rather than searching nearest neighbor from the entire image. The column-wise feature descriptors consider

localized regions in which SPM helps to reduce adverse influence of rotational variations. This approach therefore allows better consideration of local pixels/pattern matching for superior cross domain matching. A convex optimization problem is formulated by introducing the constraints to minimize the large margin among the intra-class variances [12]. The extended NBNN-based domain adaptation learns a Mahalanobis metric for each class in order to classify the images into different categories. A significant improvement in the cross-domain iris recognition accuracy is observed from the experimental results presented in this paper. This method performs particularly well when the intra-class variations are significantly higher. It is primarily due to this fact that the cross-spectral iris recognition using this approach achieves (section VII-C) better performance when compared to the cross-sensor iris recognition. We also develop an iris texture synthesis framework, using multiscale Markov random fields (MRF) model, to achieve superior cross-domain iris matching capability.

The key contribution of this paper can be summarized as follows:

1) A robust and meaningful domain adaptation strategy requires effective learning of representative features from the registration or training data. Such learning can be achieved using real-valued feature representation, rather than using binary features or iris codes that are commonly used for iris recognition. This is the key reason that most of the previous approaches, like in [13], used Mahalanobis distance metric during domain adaptation strategy. Therefore, a new similarity measure based on real-valued representation is proposed in section III, which performs almost same as those using popular binarized iris codes for same sensor iris data, but unlike binary codes the feature representation can be adopted for the domain adaptation learning. A classification framework based on NBNN domain adaptation (section IV) and MRF model (section V-A) is proposed in this paper for more accurate cross-domain iris recognition. Our experimental results in section VII on three publicly available databases suggests significant performance improvement for matching cross-domain iris images.
2) This paper also proposes and evaluates a new class of bi-spectral iris recognition system that can simultaneously acquire visible and near infra-red images. Our experimental results presented in this paper on the data of 280 sufficient classes illustrate that the combination of simultaneously acquired iris image samples can significantly improve the matching performance that may not be possible by conventional NIR-based iris recognition or visible illumination based iris recognition alone. Major problem for the bi-spectral imaging is the lack of pixel correspondence from the images acquired under two different wavelengths. This paper details on addressing such challenges and presents outperforming experimental results from the simultaneously acquired bi-spectral images.
3) In the best of our knowledge, there is no publicly available database which has exact pixel correspondence to study the cross-spectral iris recognition problem. We describe the development of such cross-spectral iris image database which can enable simultaneous acquisition of iris images, under the visible and near infra-red illumination, which can provide more accurate representation of cross-spectral iris information. This paper provides such database of cross-spectral iris images, acquired from 209 subjects, in the public domain [14] to further advance research in this area.

### A. Related work

The cross-domain iris recognition problem can categorized into two sub-categories, namely, cross-spectral and cross-sensor iris recognition. Each of these problems is briefly reviewed in the following subsections. Table I provides a summary of related iris recognition algorithms for the cross domain iris matching problem.

*1) Cross-Spectral Iris Recognition:* In the cross-spectral iris recognition, the iris images acquired under visible wavelengths are matched against the images acquired under near infra-red wavelengths. There have been recent efforts to develop cross-spectral iris recognition systems. Reference [17] describes a framework for accurately segmenting the iris images from face images acquired at-a-distance under near infra-red or visible illuminations. Very few efforts have been made to analyze the multi-spectral iris imaging. Ross et al. [18] proposed the enhanced iris recognition system by considering the fusion of multiple spectrum beyond the wavelengths of $900nm$. Recently the cross-spectral periocular matching has been explored in [19] using trained neural network. An approach for cross spectral iris matching [15] was proposed using the predictive NIR image.

*2) Cross-Sensor Iris Recognition:* Recent studies show that the iris recognition leads to reduced iris matching performance [20] when the iris sample acquired from one sensor is matched against the iris sample acquired from different sensor. For the first time, Bowyer et al., [20], [21] provided an empirical study for the sensor mismatch problem. There is limited literature in cross-sensor iris adaptation algorithms. Pillai et al. [13] proposed a framework to improve the matching performance for cross-sensor adaptation using kernel transformation learning. Xiao et al. [16] investigated an optimization model of coupled feature selection for comparing cross-sensor iris data. The optimization problem is formulated to minimize the misclassification errors and to improve the sparsity among the coupled features using $l_{2,1}$-$norm$ regularization. Connaughton et al. [21], [22] explored the cross-sensor iris recognition using the iris data acquired using three different iris cameras. Arora et al. [23] proposed a pre-processing framework to classify the iris cameras in order to address the issue of sensor interoperability. Face images can be directly matched with periocular images and such attempt is detailed in reference [24]. Gil Santos et al. [25] introduced a cross-sensor iris and periocular dataset using 10 different mobile setups for data acquisition. These authors have suggested combining the simultaneously acquired iris and periocular information to address recognition challenges for iris recognition under mobile imaging environments.

TABLE I
SUMMARY OF RELATED WORK ON DIFFERENT CROSS DOMAIN IRIS MATCHING

| Ref. | Method | Iris comparisons | Employed-database (# of images / classes) | Feature extraction | % Recognition (Non-Adapted) | rate (Adapted) |
|---|---|---|---|---|---|---|
| [15] | A predictive NIR iris image is used from the color image | Cross-spectral | WVU Multi-spectral iris database (232 images/68 classes) | log-Gabor | 100 (FAR=0.1) | 100 |
| [13] | A sensor adaptation algorithm is proposed for cross-sensor iris recognition using kernel transformation learning. | Cross-sensor | BTAS 2012 Cross-sensor iris competition database (UND dataset) | log-Gabor | 78.14 (FAR=0.1) | 82.89 |
| [16] | An optimization model of coupled feature selection is proposed for comparing cross-sensor iris data | Cross-sensor | UND dataset (14000 images/700 classes) | Ordinal measures | 94 (FAR=0.1) | 96 |
| **This paper** | NBNN-based domain adaptation between two different iris sensors' data | Cross-sensor | (a) IIITD Contact Lens Iris database (1270 images/127 classes) | Real-valued log-Gabor phase | 84 (FAR=0.1) | 89.92 |
| | | | (b) UND dataset (6420 images/214 classes) | | 87 (FAR=0.1) | 87.7 |
| **This paper** | (a) NBNN-based domain adaptation for cross-spectral iris recognition | Cross-spectral | PolyU bi-spectral iris database (8,400 images/280 classes | Real-valued log-Gabor phase | 41.88 (FAR=0.1) | 58.8 |
| | (b) NIR to VIS texture synthesis using MRF model | | | | 41.88 (FAR=0.1) | 61.9 |

### B. Domain Adaptation

The domain adaptation generally refers to the mismatch between the data acquired from two different domains. Recently, domain adaptation has gained much attention from researchers [26], [27]. Gopalan et al. [26], [28] proposed the adaptation algorithm by projecting the samples of both the domains onto different intermediate subspaces and utilized the Grassmann manifold, for calcuating a 'shortest' geodesic path between such domains. Gong et al. [29], [30] describe unsupervised learning of a geodesic flow kernel (GFK) and supervised learning of multiple base GFKs in order to project the domains onto infinite number of subspaces. In [27], a transformation learning is applied to map the source to target domain data using information theoretic learning. Also different novel adaptation approaches for classification appears in [31]-[32]. Few techniques use spatial pyramid matching for in-domain classification problems [11], but not for cross-domain problems.

The rest of the paper is organized as follows: in section II, the proposed solution for cross-domain iris recognition is depicted in a simplified block diagrams. In section III, a real-valued feature extraction method is proposed. In section IV, the details about NBNN-based domain adaptation and the extended DA-NBNN classification framework are presented. The texture synthesis approach for conversion of near infrared to visible image patches using MRF model is explained in section V. Iris recognition using Bi-Spectral Imaging is described in section VI. The proposed algorithms is evaluated on standard cross-domain iris data in section VII. Finally, key conclusions from this paper are summarized in section VIII.

## II. Block Diagram of Proposed Solution

A simplified block diagram of the proposed iris classification framework investigated in this paper is illustrated in Figure 1. The framework accepts the respective cross-domain iris image data either from cross-spectral or from cross-sensor iris data acquisition. The iris segmentation, normalization and template extraction are performed for both iris images of two domains using the algorithm in [33]. The segmentation parameters of the NIR iris image is applied on visible (R-channel) iris image in order to segment the iris region. The binary iris code is extracted and converted to real-valued local feature descriptor which is proposed in this paper. A classification framework based on the NBNN-based domain adaptation is then applied to achieve superior matching performance for the cross-spectral as well as cross-sensor iris recognition problem.

## III. Real-valued Feature Representation for Iris Similarity Measure

A robust and meaningful domain adaptation strategy requires effective learning of representative features from the registration or training data. Such learning can be effectively achieved using real-valued feature representation, rather than using binary features or iris codes that are commonly used for iris recognition. This is the key reason that some of most promising approaches, like in [13], used Mahalanobis distance metric during domain adaptation strategy.

Therefore, a new similarity measure based on real-valued representation of log-Gabor filter responses is investigated in this paper. This measure performs almost same as those using popular binarized iris codes while matching same sensor iris data, but unlike binary codes the proposed feature representation can be adopted for domain adaptation learning. We firstly define the notations used in this paper.

*a) Notations:* Let $\Theta_i$ be the set of local feature descriptors extracted from the normalized iris image $i$ having width $w$ and height $h$.

$$\Theta_i = \{\theta_{i_1}, \theta_{i_2}, ..., \theta_{i_P}\},\ \forall \theta_{i_p} \in \mathbb{R}^d \tag{1}$$

where $p = \{1, 2, ...P\}$ and $d$ is the length of feature descriptor. When there is no noise (e.g., occlusions, shadows, etc...)

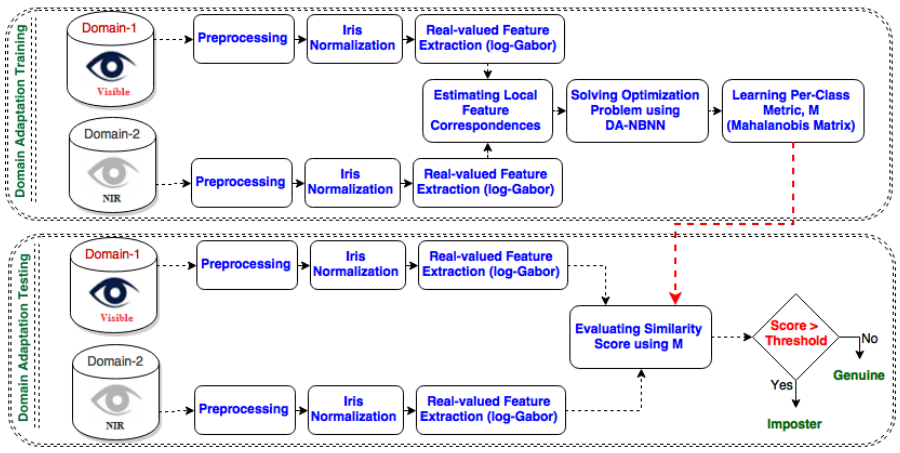


Fig. 1. Block-diagram of the proposed DA-NBNN-based iris classification framework

in the unwrapped iris image, then $P = w$ and $d = h$. In presence of noise from real life iris images, the number of local feature descriptors ($P$) becomes $(w - n)$, where $n$ represents the number of noisy feature descriptors. The noisy feature descriptors are expected to be ignored during the adaptation. The feature descriptor, $\theta_w$ can be represented as $[r_{1w}, r_{2w}, r_{3w}, ..., r_{hw}]^\top$.

The similarity measure between two iris images $\Theta_i$ and $\Theta_j$ is defined as $Ed(\Theta_i, \Theta_j)$ and can be computed as:

$$Ed(\Theta_i, \Theta_j) = \frac{\sum_{p=1}^{(w-n_{ij})} \frac{||\theta_{i_p} - \theta_{j_p}||^2}{h}}{(w - n_{ij})} \tag{2}$$

where $n_{ij}$ is the number of all the noisy feature descriptors from both the respective normalized iris images, $i$ and $j$. The equation 2 can be written as follows:

$$Ed(\Theta_i, \Theta_j) = \frac{\sum_{p=1}^{P} \frac{\sqrt{diag((\theta_{i_p} - \theta_{j_p}) M (\theta_{i_p} - \theta_{j_p})^\top)}}{h}}{P} \tag{3}$$

where $P$=$(w - n_{ij})$ and $diag(.)$ is the operator to trace diagonal elements of the matrix. If the Mahalanobis distance metric, $M \in \mathbb{R}^{d \times d}$, is an identity matrix, then the similarity measure, $Dist(\Theta_i, \Theta_j)$ can be computed using the average of the Euclidean distances between all the corresponding valid feature descriptors.

In this work, like most of other work in the literature [13], [5], the feature descriptor for iris recognition is computed using the 1D log-Gabor filter response. The frequency response of the filter can be defined as follows:

$$G(x) = e^{-\frac{1}{2}(log(\frac{x}{x_0})/(log(\frac{\sigma}{x_0}))^2} \tag{4}$$

where $x_0$, $\sigma$ are the centre frequency and bandwidth of the filter, respectively. The 1D log-Gabor filter is convolved with each row of normalized iris image ($i$) which generates the complex response $(a + jb)$ for each pixel in $i$. The real ($a$) and imaginary ($b$) values of the complex number is typically quantized into either 0 or 1 based on sign of the response values. However, in our approach this complex value is converted into real value as follows:

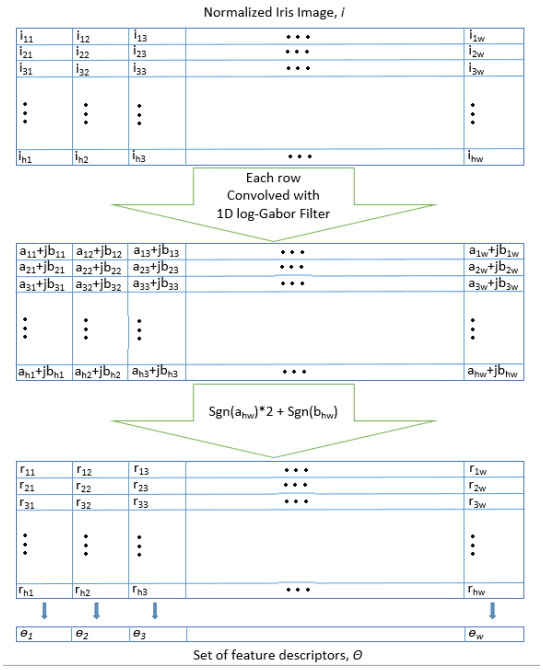


Fig. 2. Real-valued feature extraction from normalized iris image using 1D log-Gabor filter, $\theta_w = [r_{1w}, r_{2w}, r_{3w}, ..., r_{hw}]^\top$

$$a + jb \iff sgn(a) * 2 + sgn(b) \tag{5}$$

where $sgn(.)$ operator generates either 1 (if value is positive) or 0 (if value is negative). The feature descriptor is constructed using such real values considered column-wise to form a vector of size, $h \times 1$. This procedure is graphically illustrated as shown in Figure 2.

## IV. NBNN-based Domain Adaptation

This section provides a brief review on the NBNN framework for defining domain adaptation using the optimization problem formulated in equation 10. We then describe the metric learning which is used for solving the optimization problem in

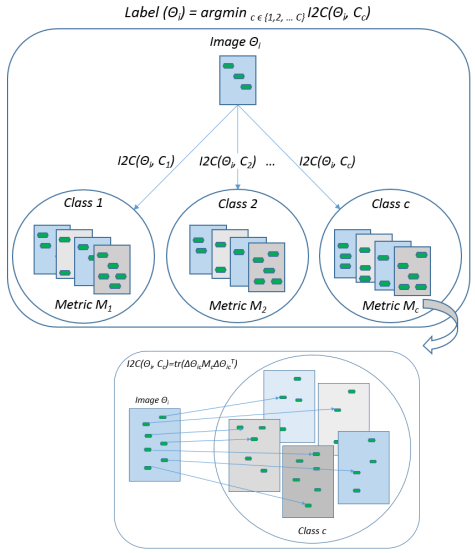


Fig. 3. NBNN classification framework using the I2C distance and the learned Per-Class metric (Mahalanobis distance). Circles and rectangles represent the class labels and images, respectively. Local feature descriptors are illustrated as green colored points.

DA-NBNN framework. Let the source iris samples available be denoted by $S = \{(\Theta_1, y_1), (\Theta_2, y_2), ..., (\Theta_L, y_L)\}$ and $y_l$ are the labeled classes where, $l = \{1, ...L\}$. Also the target iris samples with unlabeled classes are available as target set $T = \{\Theta_u\}_{u=1}^{U}$.

As shown in Figure 3, the NBNN classifier uses image-to-class (I2C) distance based on learned Mahalanobis distance metric for each class. The I2C distance between the image $\Theta_i$ and the class $c$ can be defined as follows:

$$I2C(\Theta_i, c) = \frac{\sum_{p=1}^{P} \frac{||\theta_{i_p} - \theta_{i_p}^c||^2}{h}}{P} \tag{6}$$

where $\theta_{i_p}^c$ is the local feature descriptor which is close to $\theta_{i_p}$ among all the feature descriptors in class $c$. For each descriptor of the image looks for the closest of all the feature descriptors of all members of that particular class. Therefore each input image considers all members for finding the closest feature descriptor for this class. The metric learning of Mahalanobis distance, $M_c \in \mathbb{R}^{d \times d}$ will be explained in section IV-A. The learned I2C distance can be expressed as:

$$I2C(\Theta_i, c) = \frac{\sum_{p=1}^{P} \frac{\sqrt{diag((\theta_{i_p} - \theta_{i_p}^c) M^c (\theta_{i_p} - \theta_{i_p}^c)^\top)}}{h}}{P} \tag{7}$$

For notational simplicity the I2C distance can be written as follows:

$$I2C(\Theta_i, c) = Dist(\triangle\Theta_{i_c} M_c \triangle \Theta_{i_c}^\top) \tag{8}$$

where $\triangle\Theta_{i_c} = [(\theta_{i_1} - \theta_{i_1}^c)^\top (\theta_{i_2} - \theta_{i_2}^c)^\top ... (\theta_{i_p} - \theta_{i_p}^c)^\top]^\top$ and $Dist(.)$ is the function of Euclidean distance. The image class labels can be identified using the positive $I2C$ distance which can be calculated as:

$$p = \underset{c}{\operatorname{argmin}}\, I2C(\Theta_i, c) \tag{9}$$

All the distances to other classes can be considered as negative $I2C$ distances, $n$.

### A. DA-NBNN Metric Learning

The large variations in iris similarity scores from the cross-domain iris matching can be attributed to the mismatch of imaging wavelengths, illumination, and optical lens. Even under such frequently observed variations in the cross-domain iris images, the local feature descriptors across the two domains are expected to be correlated and such similarity can be further improved by domain adaptive NBNN (DA-NBNN) framework. Keeping these aspects in mind, we can formulate an optimization problem using the methods described in [8], [10]. This convex optimization problem can be formulated with respect to two iris imaging domains, namely, source $s$ and target $t$ as follows:

$$\min_{M_1, M_2, ..., M_c} O(M_1, M_2, ..., M_c)^k = \tag{10}$$

$$\gamma_s^k \left[ (1 - \lambda_s) \sum_{l,p \to l} Dist(\Delta\Theta_{lp} M_p \Delta\Theta_{lp}^T) + \lambda_s \sum_{l,p \to l}^{n \to l} \xi_{lpn} \right]^k +$$

$$\gamma_t^k \left[ (1 - \lambda_t) \sum_{u,p \to u} Dist(\Delta\Theta_{up} M_p \Delta\Theta_{up}^T) + \lambda_t \sum_{u,p \to u}^{n \to u} \xi_{upn} \right]^k$$

$$s.t. \forall \{l, p, n\}_s : n - p > 1 - \xi_{lpn}, \xi_{lpn} > 0$$
$$and\ \forall \{u, p, n\}_t : n - p > 1 - \xi_{upn}, \xi_{upn} > 0$$
$$and\ \forall c : M_c \succeq 0$$

where $\lambda_s$ and $\lambda_t$ are the two trade-off parameters to regularize the given constraints for minimizing the positive distances between the source and target, respectively. $M_c$ is said to be positive semi-definite. $\gamma_s^k$ and $\gamma_t^k$ are the relative weights given at each iteration, $k$. The solution for this optimization problem can be obtained in a similar manner as described in [10]. After learning the Mahalanobis metrics for each class, the NBNN classifier is used to classify the images across two different domains.

### B. Extended DA-NBNN Framework

In this framework, the DA-NBNN is extended to improve the cross-domain iris matching capability by adopting the idea of spatial pyramid match (SPM)[11]. The solution may not be suitable for the standard testbed used for visual domain adaptation methods, because the region of interest in the source image can be significantly different from the image in target domain. But this formulation is more suitable for the cross-domain iris mismatch problem, as such variations among the spatial coordinates for local iris feature descriptors are expected to be small as the iris normalization steps helps to limit such variations. However, there are other challenges due to noise introduced by the specular reflections, eyelashes

and pupil dilation and contractions. These challenges can be handled while normalizing the iris images.

The SPM divides the image into different blocks at different levels of fine resolution and finds the similarity between the corresponding blocks in candidate class rather than searching the NN from the whole image of that particular class. The column-wise feature descriptors consider localized regions in which SPM helps to reduce adverse influence of rotational variations. The proposed framework uses the level-1 blocks from which the local feature descriptors are extracted. The noisy blocks are discarded and rest of the blocks are considered for the domain adaptive NBNN with SPM, also named as Extended DA-NBNN framework.

The steps involved in extended DA-NBNN algorithm are summarized in Algorithm 1. The sample local feature descriptors are considered from two different iris domains to define the source and target sets, $S_k$ and $T_k$, respectively. These sets are split into $Q$ subsets. For each subset the source and target samples are defined as $S_k^b$ and $T_k^b$. At each iteration $k$, the labels for all the samples will be predicted by minimizing the image-to-class distance. Mahalanobis matrices $M_{b_{k+1}}^c$ and the sample data sets, $S_{k+1}$, $T_{k+1}$ and $U_{k+1}$ will be updated block-wise by solving the optimization problem defined in equation (10). Finally, the target labels are calculated by considering the mode of block-wise class labels.

**Algorithm 1:** Extended DA-NBNN

**Input:** $S = \{(\Theta_1, y_1), (\Theta_2, y_2), ..., (\Theta_L, y_L)\}$,
$S^b = \{(\Theta_{l_b}, y_{l_b})\}_{l=1}^{L},\ b = \{1, ...Q\}$
$T = \{\Theta_1, \Theta_2, ..., \Theta_U\}$
$T^b = \{\Theta_{u_b}\}_{u=1}^{U},\ b = \{1, ...Q\}$

**Output:** $y_u, \forall u \in T$

**for** *each block, b=1 to Q* **do**
  `Initialize` $S_0^b = S^b,\ T_0^b = \emptyset,\ U_0^b = T^b,\ M_{0b}^c = I$
  **for** *iteration, k=1 to K* **do**
    `Solve` $\forall u_b \in U_k^b,\ y_{u_b} = \underset{c}{\operatorname{argmin}}\, I2C(\Theta_{u_b}, c)$;
    with $\theta_{u_b p}^c \in (S_k^b + T_k^b), \forall p \in \{1, ..., P_{u_b}\}$
    `Calculate` $\forall l_b \in S_k^b,\ I2C(\Theta_{l_b}, c)$
    with $\theta_{l_b p}^c \in (S_k^b + T_k^b - l), \forall p \in \{1, ..., P_{l_b}\}$
    `Update` $S_{k+1}^b,\ T_{k+1}^b,\ U_{k+1}^b$
    `Solve` the optimization problem given in equation (10), for finding $M_{b_{k+1}}^c$
Find the target labels, $y_u$

## V. Near Infrared to Visible Iris Synthesis

All the iris images from near infrared and visible wavelengths are aligned during the imaging in such a way that the spatial locations of the corresponding pixels in both near infrared and visible iris images are same. The normalized iris image region is divided into blocks with overlapping neighboring patches. For each patch on the input near infrared normalized iris image, the patch in the corresponding visible normalized iris image is estimated. In order to estimate the visible iris image patch $\theta_j^{vis}$ of the input near infrared iris image patch $\theta_j^{nir}$; $K$ candidate visible normalized iris image patches $\left\{\theta_j^{vis}{}^l\right\}_{l=1}^{K}$ are acquired from the training set. The synthesized visible iris image should closely match the input near infrared iris image in appearance and be smooth in the meanwhile. In order to achieve this objective, a Markov network is used to model the process of visible iris texture synthesis.

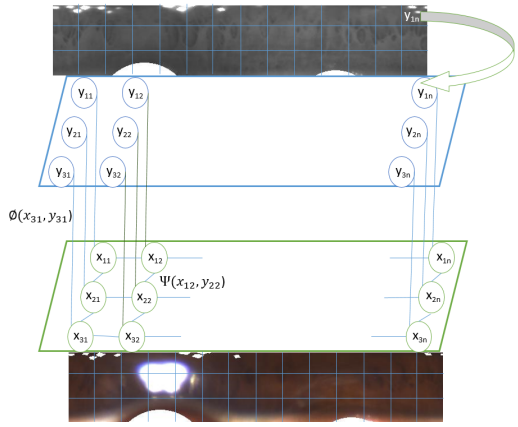


Fig. 4. Markov network for infra-red and visible iris image patches where $\theta^{nir} = y_{ij}$ and $\theta^{vis} = x_{ij}$, $x_{ij}$ means the $i^{th}$ row and $j^{th}$ column of visible iris image patches and $y_{ij}$ means the $i^{th}$ row and $j^{th}$ column of near infra-red iris image patches.

### A. Cross-Spectral Iris Recognition using MRF model

The graphical model of Markov network can be constructed for generalized low-level vision problems [34], [35], [36]. Such model is shown in Figure 4 and can be used to identify solutions in two key phases, namely, $learning$ and $inference$. In $learning$ phase, the network parameters will be trained until some optional solution is reached, whereas in $inference$ phase, the patches for the visible iris image are estimated.

The joint probability of visible ($\Theta^{vis}$) and near infra-red ($\Theta^{nir}$) iris image patches for a Markov random field can be defined as follows:

$$\begin{aligned} &P(\Theta^{vis}, \Theta^{nir}) \\ &= P(\theta_1^{vis}, \theta_2^{vis}, ..., \theta_N^{vis}, \theta_1^{nir}, \theta_2^{nir}, ..., \theta_N^{nir}) \\ &= \prod_{(i,j)} \Psi(\theta_i^{vis}, \theta_j^{vis}) \prod_k \Phi(x_k, \theta_k^{nir}) \end{aligned} \tag{11}$$

where $\theta_i^{vis}$ has $K$ possible states which are determined from the candidate visible iris image patches. The compatibility function between visible iris image patches can be computed as,

$$\Psi(\theta_k^{vis.l}, \theta_j^{vis.m}) = e^{-|d_{jk}^l - d_{kj}^m|^2 / 2\sigma_{vis}^2} \tag{12}$$

where $k$ and $j$ are two neighboring visible iris image patches with a region of overlapping and $d_{jk}^l, d_{kj}^m$ represent the intensity values of the overlapping region between the $l^{th}$ and $m^{th}$ candidate visible iris image patches. The $\sigma_{vis}$ represents the covariance of Gaussian noise which is employed to differentiate the training data of visible iris images from the $ideal$ training data.

The local evidence can be computed as follows:

$$\Phi(\theta_k^{vis.l}, \theta_k^{nir}) = e^{-|\theta_k^{nir.l} - \theta_k^{nir}|^2 / 2\sigma_{nir}^2} \tag{13}$$

$\sigma_{nir}$ is the Gaussian noise of covariance used to differ training data of near infra-red iris images from the $ideal$ training data and $\theta_k^{vis.l}$ represent $l^{th}$ candidate visible iris image patch.

In the $learning$ phase of Markov network, unknown parameters can be computed from the solution of the following problem:

$$\hat{\theta^{vis}}_{j\ MAP} = \underset{\theta_j^{vis}}{\operatorname{argmax}} \max_{all\ \theta_i^{vis}, i \neq j} P(\theta_1^{vis}, \theta_2^{vis}, ..., \theta_N^{vis}, \theta_1^{nir}, \theta_2^{nir}, ..., \theta_N^{nir}) \tag{14}$$

where $\hat{\theta^{vis}}_{j\ MAP}$ is the MAP estimate for computing maximum of marginal probabilities of all visible image patches.

In the $inference$ phase, belief propagation [36] is used to achieve optimal solution for the Markov network. Such propagation is achieved with the passing of local $messages$ between the neighboring patches (or network nodes) in order to compute the MAP estimate. The MAP estimate for visible iris image patches can be rewritten as follows:

$$\hat{\theta^{vis}}_{j\ MAP} = \underset{\theta_j^{vis}}{\operatorname{argmax}}\, \Phi(\theta_j^{vis}, \theta_j^{nir}) \prod_k M_j^k \tag{15}$$

Belief in patch $j$, is defined as the product of all local evidences from visible iris image patches and the messages entering into that $j^{th}$ visible iris image patch. The message passes from node $k$ to $j$ can be represented as follows:

$$M_j^k = \max_{[\theta_k^{vis}]} \Psi(\theta_j^{vis}, \theta_k^{vis}) \Phi(\theta_k^{vis}, \theta_k^{nir}) \prod_{l \neq j} \hat{M}_k^l \tag{16}$$

The propagation rules in equation 16 are applied in order to get the optimal solution of Markov random fields. The network is trained using equation 14 and the updated unknown parameters are employed to recover corresponding patches from near infrared image patches to synthesize visible patches for the matching.

## VI. Iris Recognition using bi-spectral Imaging

Iris images are believed to be highly unique [1], [2] and reveal different information when viewed under different illumination or wavelengths. Several studies [37], [38], [4] on iris recognition under visible wavelengths have shown promising results. Therefore one of our objective in this work has been to evaluate simultaneous recovery and matching of iris images under visible and near-infrared illumination to achieve higher accuracy that may not be possible by any of these approach individual. We developed a low-cost imaging setup that can simultaneously acquire near-infrared and visible wavelength iris images in single shot. Figure 5 illustrates block diagram of such simultaneous imaging which can not only develops more accurate iris imaging but also develop a unique dataset with exact pixel correspondence which is required by the biometrics community to study cross-spectral iris recognition capabilities. The setup detailed in Figure 5 simultaneously acquires iris images under both visible and near-infrared wavelengths. The mechanism for the precise separation of visible and near infrared images of the spectrum is also illustrated in Figure 5. In order to meet the requirement, bi-spectral imaging approach is selected which utilizes a dichroic prism that can accurately segregate incoming images for the visible sensor and the other one for the near infrared sensor/camera. Acquired visible and near infrared images are of same size, i.e., 640 $\times$ 480 pixels. Selecting appropriate illumination sources for both the spectrum is significant for high quality of visible and near infrared imaging. In order to acquire the good quality iris images, the factors like exposure, gain and illumination intensity are independently considered for both the channels.

TABLE II
Imaging parameters for the visible and near infra-red channels

| Variable | Near infra-red channel | Visible channel |
|---|---|---|
| Exposure limit value ($\delta_e$) | 15 | 150 |
| Gain limit value ($\delta_g$) | -80 | 75 |
| Illumination intensity ($E_{IR}$) ($W/m^2$) | 2.6 | 2.123 |
| Illumination angle ($degrees$) | 60 | 45 |

The camera specifies that the exposure limits ($\delta_e$) ranges from 0 to 792 and the gain limits ($\delta_g$) ranges from -89 to 593. After analyzing different exposure and gain combinations, the settings for both the channels are finalized empirically as shown in Table II. In visible channel, the exposure and gain settings are fixed as 150 and 75, respectively. The illumination source used for the visible channel is a professional video light (VL-S04) whose illumination intensity is 1450Lux and the illumination angle is 45 degrees. In similar way, the exposure and gain parameters were fixed as 15 and -80, respectively, for the near infra-red channel. The near infra-red illumination can cause damage to the eye if its intensity exceeds some limit. In order to alleviate near infra-red radiation hazard, a ring illuminator is specifically designed which is suitable for the proposed acquisition environment. The total IR illumination intensity of 2.6W is used at a distance of 10 cm from ring illuminator to the eye. The setup can simultaneously acquire iris images from both the channels and store the images as well as the sequence of different images at an interval of 0.5 seconds for further investigation. The sample iris images acquired as bi-spectral imaging for both right and left eyes using the proposed acquisition setup are illustrated in Figure 6.

## VII. Experiments and Results

In this section, we firstly describe the databases for performing the experiments to validate the approach detailed in section IV-B. Then the proposed domain adaptation algorithm is evaluated using the real-valued feature descriptors extracted from these datasets. Iris recognition using simultaneous imaging of iris using two domains is also evaluated and discussed in section VII-F.

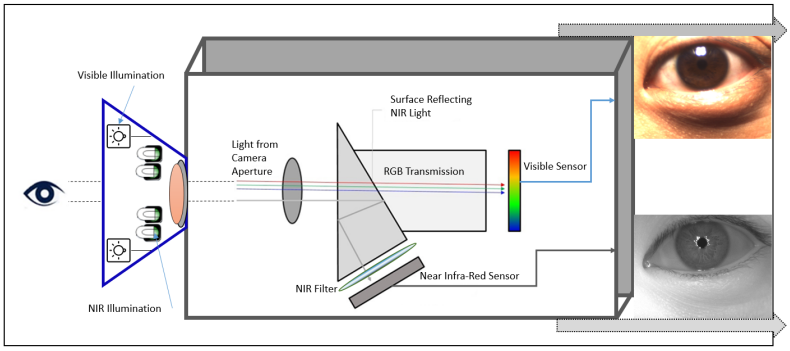


Fig. 5. Simultaneous iris imaging under near infrared and visible illumination

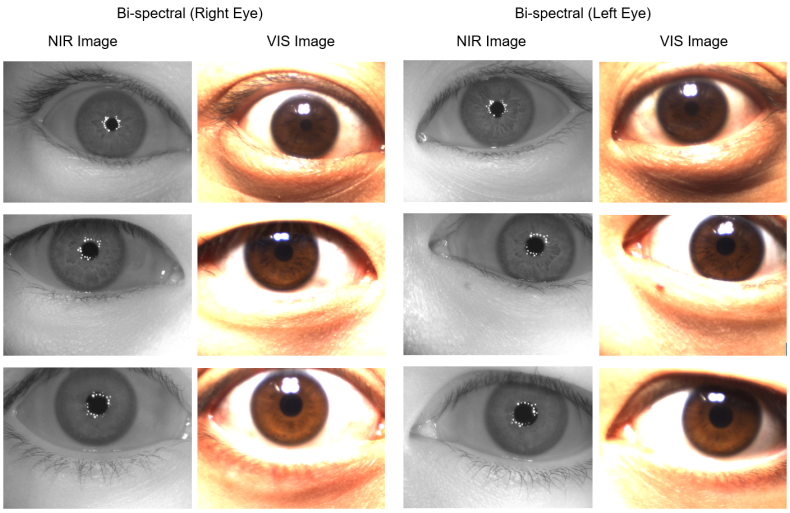


Fig. 6. Simultaneously acquired sample iris images under near infrared and visible wavelengths with full pixel correspondences

### A. Datasets

The cross-domain experiments are firstly performed using two publicly available cross-sensor iris datasets, namely, IIIT-D CLI database [39], [40], ND Cross sensor 2012 iris database [41] and the PolyU cross-spectral iris database[14]. We briefly describe these datasets in the following:

*1) IIIT-D Contact Lens Iris (CLI) database:* IIIT-D CLI database has iris images acquired using two different iris sensors, namely, Cogent dual iris sensor (CIS 202) and VistaFA2E single iris sensor. The iris samples are captured from 101 subjects, both left and right iris images. Although this database was developed for the evaluation of iris recognition performance using contact lenses, it also provides images without contact lenses that are acquired from different iris sensors. Therefore this publicly available dataset can also be used for the cross-domain iris recognition performance and used in our experiments. There are 1270 properly segmented iris images from 127 classes with 5 instances, each from both the iris sensors.

*2) ND Cross-Sensor Iris 2012 dataset:* The university of Notre Dame cross-sensor iris dataset was acquired at Notre Dame and firstly used for BTAS 2012 competition [41]. Two sensors, namely LG4000 and LG2200, were used to acquire the iris image database. There are 676 unique subjects participated across 27 sessions with total number of 29,939 iris images with LG4000 and 117,503 iris images with LG2200. Due to the limited computational resources, only 214 different classes are chosen randomly with each class having 15 instances from both the sensors.

*3) PolyU Cross-Spectral Iris Database:* This is a unique bi-spectral iris image dataset developed to study cross-spectral iris recognition and is made publicly available, see [14]. This database of iris images has been acquired under simultaneous bi-spectral imaging, from both right and left eyes, using the acquisition setup that is being developed as illustrated in Figure 5. This database consists of total 12,540 iris images ($209 \times 2 \times 2 \times 15$) which are acquired with 15 instances from 209 different subjects. Each of the iris images are of $640 \times 480$ pixels size and with pixel correspondences in both the near-infrared and visible iris images.

### B. Cross-Sensor Iris Recognition using DA-NBNN

In order to evaluate the cross-sensor iris recognition performance, first two databases described in above section were used. The experimental results using IIIT-D database are presented on 1270 iris images which are properly segmented from 127 classes with 5 instances each from both the iris sensors. Similar to as in [13], we also employed 214 classes

TABLE III
CROSS-SENSOR IRIS RECOGNITION PERFORMANCE USING IIITD CLI DATABASE

| Iris comparisons | EER | Recognition rate (%) at 0.1 FAR |
|---|---|---|
| Cogent vs. Vista (Non-Adapted) | 14.39 | 84 |
| Cogent vs. Vista (Adapted) | 10.02 | 89.92 |

TABLE IV
CROSS-SENSOR IRIS RECOGNITION PERFORMANCE USING ND DATABASE

| Iris comparisons | EER | Recognition rate (%) at 0.01 FAR |
|---|---|---|
| Non-Adapted | 8.6 | 79.13 |
| Adapted | 7.9 | 83.83 |

from UND dataset and each of these classes have 15 instances from both the iris sensors.

*1) IIITD CLI database:* The cross-sensor iris recognition performance is evaluated using DA-NBNN framework. We present the ROC curves for cross-sensor iris recognition on IIITD CLI database as shown in Figure 7(a). The equal error rate (EER) and the genuine acceptance rate at FAR of 0.1 are provided in Table III. The CMC curves for cross-sensor iris recognition on IIITD CLI database are shown in Figure 7(b). The experimental results illustrate significant improvement in the cross-sensor iris recognition performance over baseline performance.

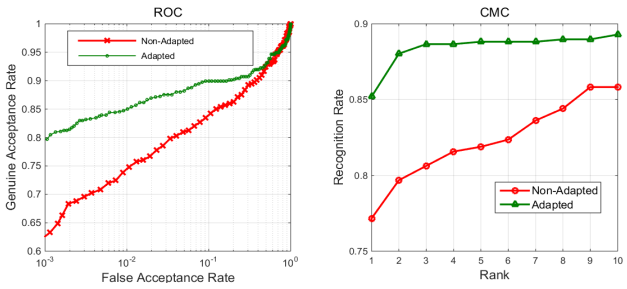


(a) (b)

Fig. 7. IIITD CLI database (a) ROC curve for iris cross-comparisons using DA-NBNN, (b) CMC curve for iris cross-comparisons using DA-NBNN

*2) ND cross-sensor iris 2012 dataset:* In this section, we present the ROC curves for cross-sensor iris recognition on ND dataset as shown in Figure 8(a). Table IV illustrates the comparative EER and the genuine acceptance rate at 0.01% of FAR The CMC curves for cross-sensor iris recognition on ND dataset are shown in Figure 8(b). These results demonstrate that there is significant improvement in the cross-sensor iris recognition performance.

### C. Cross-Spectral Iris Recognition using DA-NBNN

Iris images from all the subjects in PolyU cross-spectral database were utilized for the feature extraction and evaluation.

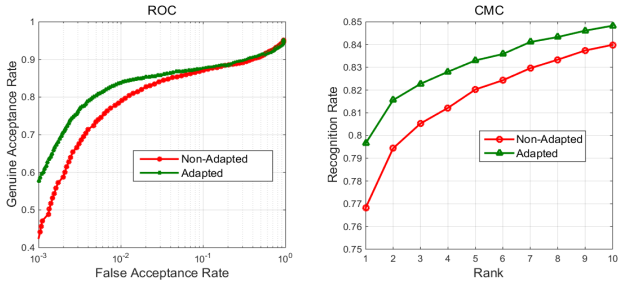


(a) (b)

Fig. 8. ND database (a) ROC curve for iris cross-comparisons using DA-NBNN, (b) CMC curve for iris cross-comparisons using DA-NBNN

The iris segmentation, normalization and image enhancement are performed for both NIR and VIS images (see Figure 9) using the algorithm in [33]. The segmentation parameters of the NIR iris image are directly used to segment corresponding iris region images from the visible (R-channel) spectrum iris images. This set of experiments were performed on iris images from 280 different classes (a total of 8400 images) which were properly segmented in visible and nearinfrared channels. The binary iris code extracted from normalized iris image is converted to real-valued feature vector as detailed in section III.

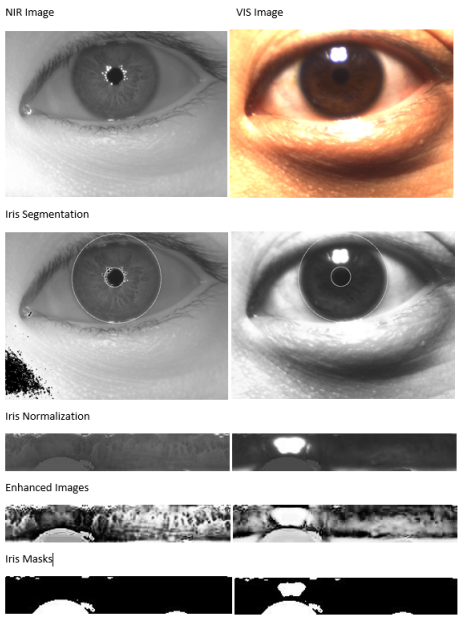


Fig. 9. Preprocessing steps for cross spectral iris recognition

The matching accuracy for the cross-spectral iris matching is ascertained from the equal error rate and the receiver operating curve. The total number of genuine and imposter comparisons are 2800 and 1953000, respectively. From Figure 10, it can be observed that even though the cross comparisons in near infra-red and visible channels are independently quite accurate, the performance of cross-spectral iris matching has significantly gone degraded. The equal error rate (EER) for near infra-red iris comparisons is 3.97% and for visible

iris comparisons is 6.56%. Where as, for cross-spectral iris comparisons, it is observed that the EER increased by 33.89%. After applying domain adaptation, the cross-spectral iris recognition performance is improved by 58.8% as shown in Table V. The EERs for all experiments on cross-sensor and cross-spectral iris databases using proposed adaptation strategies are shown in Table VI.

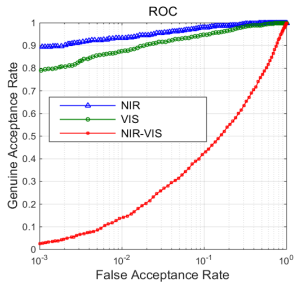


Fig. 10. The ROC curve for cross-spectral iris recognition (NIR-to-NIR; VIS-to-VIS and NIR-to-VIS comparisons)

The cross-spectral iris recognition performance is evaluated using DA-NBNN framework. The ROC curves for cross-spectral iris recognition on PolyU database are shown in Figure 11(a). The CMC curves for cross-spectral iris recognition on PolyU database are shown in Figure 11(b). The results clearly depicted significant improvement in the cross-spectral iris recognition performance.

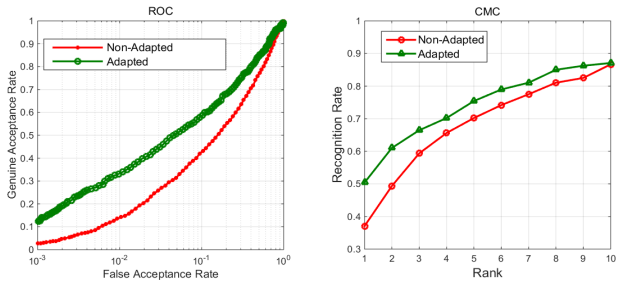


(a) (b)

Fig. 11. PolyU cross-spectral iris database (a) ROC curve for iris cross-comparisons using DA-NBNN, (b) CMC curve for iris cross-comparisons using DA-NBNN

### D. Cross-Spectral Iris Recognition using MRF

The domain adaptation method utilizes the final match score distributions of both the near infrared and visible spectrums. It may not be certain in all times that all the genuine scores have true accepts and similarly all true rejects in imposter scores. Therefore, as detailed in section V-A, more reliable approach for cross-spectral iris recognition system based on multi-scale Markov random fields was also investigated. The ROC curves for cross-spectral iris recognition on PolyU database using this approach are shown in Figure 12. The results demonstrate that there is significant improvement in the cross-spectral iris recognition performance, (61.9%) when compared to the performance from DANBNN framework (the rank-one recognition rate is 58.8% as shown in Figure 11(a)).

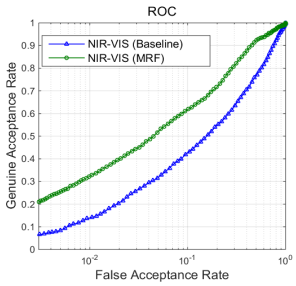


Fig. 12. The ROC curve for cross-spectral iris recognition using MRF model

### E. Comparison with Other Competing Feature Extraction Methods

In order to comparatively evaluate the proposed approach for recovering iris features for the cross-spectral iris recognition, a range of competing feature extractors were selected. Therefore, the segmented iris images from above three databases were comparatively evaluated on each of these feature extractors. The proposed real-valued feature representation approach is compared with the following methods of extracting real-valued feature descriptors in order to evaluate its performance.

*a) Log-Gabor filter based phase response:* The real-valued features [13] are extracted using the phase of the 1D log-Gabor features which can be obtained from Masek's implementation [33]. The equal error rate (EER) for sensor-1 (CIS 202) iris comparisons is 9.84% and for sensor-2 (VistaFA2E) comparisons is 17.04%. Whereas, for cross-sensor iris comparisons, it is observed that the EER increased to 32.17%. The ROC curve for these comparisons is shown in Figure 13(c).

*b) Even symmetric Gabor filter:* In this section, the experiments are conducted using the real-valued features extracted with even symmetric Gabor filter [42]. The equal error rate (EER) for sensor-1 (CIS 202) iris comparisons is 10.09% and for sensor-2 (VistaFA2E) comparisons is 13.11%. Whereas, for cross-sensor iris comparisons, it is observed that the EER increased to 29.59%. The ROC curve for these comparisons is shown in Figure 13(d).

*c) Wavelet packet decomposition (WPD):* The features under this scheme are extracted from the normalized iris image which is divided into 16 equal sized blocks. Each block of the image is decomposed into three levels using Daubechies-4 (db4) wavelet decomposition. As explained in paper [43], the most effective texture information is observed from the five sub-band images ( $LL_1$, $HL_3$, $LH_3$, $HL_2$ and $HL_1LL$), where LL, HL, LH and HH represent horizontal low - vertical low, horizontal high - vertical low, horizontal low - vertical high and horizontal high - vertical high frequency information, respectively. After obtaining these components SVD (Singular Valued Decomposition) is employed to recover five SV vectors from the respective 5 sub-band images. The equal error rate (EER) for sensor-1 (CIS 202) iris comparisons is 19.47% and for sensor-2 (VistaFA2E) comparisons is 16.47%. Whereas, for cross-sensor iris comparisons, it is observed that the EER increased to 39.33%. The ROC curve for these comparisons is shown in Figure 13(e).

TABLE V
CROSS-SPECTRAL IRIS RECOGNITION PERFORMANCE USING POLYU DATABASE

| Iris comparisons | EER | GAR (%) at 0.1 FAR (Non-Adapted) | (Adapted) | (MRF Model) |
|---|---|---|---|---|
| NIR-NIR | 3.97 | 97.82 | – | – |
| VIS-VIS | 6.56 | 94.79 | – | – |
| NIR-VIS | 33.89 | 41.88 | 58.8 | 61.9 |

TABLE VI
COMPARATIVE EERS FOR THE CROSS-SENSOR AND CROSS-SPECTRAL IRIS RECOGNITION USING PROPOSED ADAPTATION STRATEGIES

| | Cross-Sensor | | | | Cross-Spectral | | |
|---|---|---|---|---|---|---|---|
| | (IIITD) (Non-Adapted) | (IIITD) (Adapted) | (ND) (Non-Adapted) | (ND) (Adapted) | (PolyU) (Non-Adapted) | (PolyU) (Adapted) | (PolyU) (MRF) |
| EER | 14.39 | 10.02 | 8.6 | 7.9 | 33.89 | 26.68 | 23.87 |

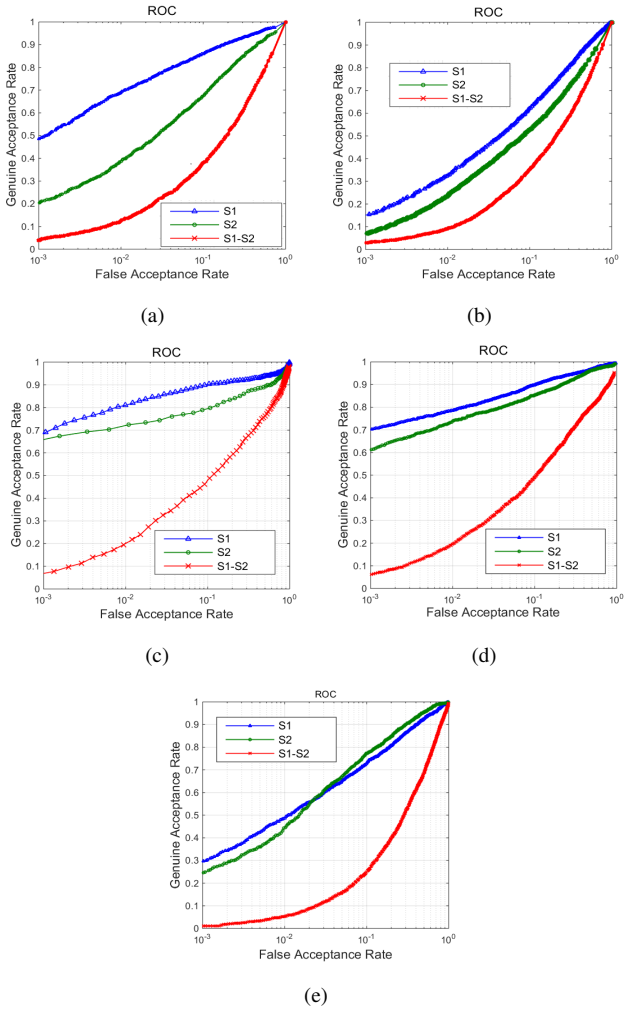


Fig. 13. ROC Curves for iris cross-comparisons: (a) SURF features (IIITD CLI), (b) SURF features (ND dataset), (c) 1D log-Gabor phase information (IIITD CLI), (d) even symmetric Gabor filter (IIITD CLI), (e) Wavelet packet decomposition (IIITD CLI).

*d) SURF features:* The features are extracted from the normalized iris image using SURF descriptors. SURF detects key-points in normalized iris image in which a circular window is constructed to estimate orientation using Haar wavelet responses in order to achieve rotation invariance. All the key-points with each key-point of length 64, forms a feature vector, say $\Theta_i$. The equal error rate (EER) for sensor-1 (CIS 202) iris comparisons is 12.36% and for sensor-2 (VistaFA2E) comparisons is 20.85%. Whereas, for cross-sensor iris comparisons, it is observed that the EER increased to 34.75%.

Another possible competing approach for cross-sensor iris recognition is to use binary features as used in [13]. However reference [13] doesn't provide adequate details to reproduce[1] the results. All implemented codes for this work are made available via reference [44]. Please see more details in Appendix A.

*e) Real-valued feature extraction:* The purpose of the experiments in this section is to ascertain the performance degradation when the real-valued features employed for domain learning are used for iris recognition from the same sensor. Therefore, the performance of cross-sensor iris recognition using the proposed approach of extracting real-valued features from the normalized iris image was also compared with conventional iriscode scheme employed for same sensor iris recognition. The equal error rate (EER) for sensor-1 (CIS 202) iris comparisons is 0.67% and for sensor-2 (VistaFA2E) comparisons is 1.94%. Whereas, for cross-sensor iris comparisons, it is observed that the EER increased to 3.29%. The comparison between the performance of binary vs. real-valued features descriptors is presented in Table VII. The ROC curves for conventional approach using iriscode and our approach using real-valued features are comparatively illustrated in Figure 14. There are 4498, 2941, 3344 genuine and 994444, 644306, 800963, impostor scores for sensor-1 (CIS 202), sensor-2 (VistaFA2E) and cross-sensor comparisons, respectively. These results suggest that the proposed real-valued feature representation performs almost as good as the binary iris codes while performance from other real-valued approaches. The iris comparisons are made for same-sensor

[1]The reproducibility of our experimental results is assured from the availability of implementation codes via reference [44].

TABLE VII
COMPARATIVE PERFORMANCE EVALUATION FOR CROSS-SENSOR IRIS RECOGNITION USING IRIS CODES AND OUR APPROACH

| Iris comparisons | EER (Iriscode) | EER (Ours) |
|---|---|---|
| Cogent vs. Cogent | 0.39 | 0.67 |
| Vista vs. Vista | 1.43 | 1.94 |
| Cogent vs. Vista | 2.96 | 3.29 |

data as well as cross-sensor iris data using IIIT-D CLI database as shown in Table VIII. The genuine acceptance rate at false acceptance rate of 0.1% is comparatively summarized in Table IX.

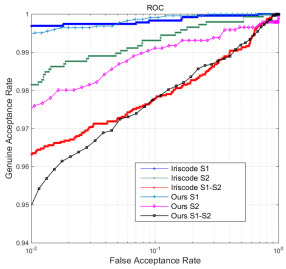


Fig. 14. Comparative ROC curves from Iriscode and Our approach

### F. Iris Recognition using Bi-Spectral Imaging

In this section, we report experimental results from the simultaneous imaging of iris under visible and near infrared illumination using the setup as detailed in section VI. The iris images from 280 different classes generated 2800 genuine and 1953000 imposter matching scores each for the visible and near infrared images. The distribution of these genuine and imposter scores from the visible and near infra-red iris images is illustrated in Figure 15(b). Each point in the scores distribution represent the match score either from genuine or imposter. The $x$-coordinate value of the point represents the match score in NIR region, whereas the $y$-coordinate value of the same point indicates the match score in VIS region. Out of the four classes of depicting genuine and imposter distribution from visible and near-infrared images, two classes for spectra are depicted on $x$-$y$ axis, and other two classes of genuine and impostor scores are shown using two different colors. The combination of these matching scores from two different spectra is expected to further improve the iris recognition accuracy. Figure 15(a) illustrates the ROC curve for different score-level weighted combinations of scores from visible and near infra-red iris images. The equal error rates for NIR and Visible (VIS) iris comparisons are 3.97 and 6.56, respectively. The weighted fusion of matching scores improved the EER to 2.86 for the weights, $w_{NIR} = 0.6$ and $w_{VIS} = 0.4$ or $(1 - w_{NIR})$, from near infra-red and visible iris images, respectively. The weighted fusion can be computed as, $w_{NIR} * Score_{NIR} + (1 - w_{NIR}) * Score_{VIS}$. Our experimental results in Figure 15(a) and Table X suggest that the combination of simultaneously acquired iris images can offer significant performance improvement over the conventional near infrared imaging based iris recognition.

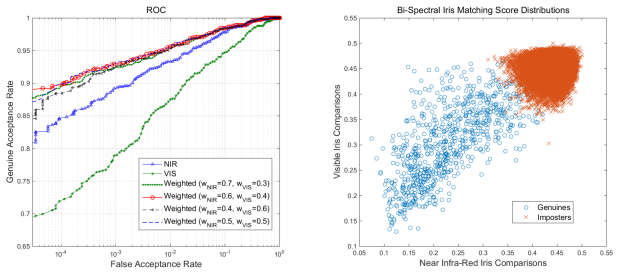


(a) (b)

Fig. 15. (a) ROC curves from simultaneous visible and near infrared iris imaging, (b) Distribution of iris match scores from two different spectra

## VIII. CONCLUSIONS AND FUTURE WORK

This paper has investigated cross-domain iris recognition problem and presented a new approach to accurately match iris images acquired under different domains. We developed an EDA-NBNN based classification framework for cross-domain iris matching. The effectiveness of the proposed approach was evaluated for cross-sensor iris matching using two publicly available databases (UND Cross-sensor iris database and IIITD CL1 iris database). This approach was also evaluated for the cross-spectral iris recognition using publicly available PolyU cross-spectral iris database. The experimental results presented in section VII-B and VII-C are outperforming and validate the cross-domain iris recognition proposed in this paper. The proposed adaptation method for cross-spectral iris recognition is capable of benefiting from the final match score distributions of both the domains, i.e. all the genuine scores that have true accepts and similarly all true rejects in imposter scores. This is the key reason for the success of proposed cross-spectral iris recognition approach based on the multi-scale Markov random fields. It can also be observed that the performance improvement for the cross-spectral iris recognition is significantly higher as compared to the performance from the cross-sensor iris recognition. Therefore it is reasonable to conclude that the proposed method can particularly perform very well when the intra-class variations among matched cross-domain iris images are high.

This paper also develops and proposes simultaneous acquisition of visible and near infrared iris images to significantly improve the iris recognition accuracy. Our experimental results presented in section VII-F validates this approach and suggests that such an approach can be used to achieve a performance that is not possible either by use of red single visible or near-infrared images alone. This paper also provides first cross-spectral iris images database [14] which has pixel-to-pixel correspondences between visible and near-infrared iris images. Availability of such database in public domain will help to advance further research and development in cross-spectral iris recognition with several emerging applications in areas like human surveillance. However, further research is required to simultaneously recover discriminant features from the periocular region that can help to further improve matching accuracy for cross-spectral iris recognition.

TABLE VIII
EERS USING IIITD CLI DATABASE FROM VARIOUS REAL-VALUED FEATURE DESCRIPTORS

| Sensor | SURF | WPD (db4+svd) | Even symmetric Gabor | 1D log-Gabor phase | **Ours** |
|---|---|---|---|---|---|
| S1 | 12.36 | 19.47 | 10.09 | 9.84 | 0.67 |
| S2 | 20.85 | 16.47 | 13.11 | 17.04 | 1.94 |
| S1 vs. S2 | 34.75 | 39.33 | 29.59 | 32.17 | 3.29 |

TABLE IX
GAR AT 0.1% FAR USING IIITD CLI DATABASE FROM VARIOUS REAL-VALUED FEATURE DESCRIPTORS

| Sensor | SURF | WPD (db4+svd) | Even symmetric Gabor | 1D log-Gabor phase | **Ours** |
|---|---|---|---|---|---|
| S1 | 86 | 73.09 | 90.02 | 90.16 | 99.9 |
| S2 | 67.76 | 77.14 | 85.35 | 79.27 | 99.1 |
| S1 vs. S2 | 38.39 | 24.43 | 49.2 | 47.71 | 97.7 |

TABLE X
COMBINED PERFORMANCE FROM SIMULTANEOUSLY ACQUIRED IRIS IMAGES USING OUR SETUP

| | NIR (Near InfraRed) | VIS (Visible) | Weighted NIR-VIS ($w_{NIR}$=0.7, $w_{VIS}$=0.3) | Weighted NIR-VIS ($w_{NIR}$=0.6, $w_{VIS}$=0.4) | Weighted NIR-VIS ($w_{NIR}$=0.4, $w_{VIS}$=0.6) | Weighted NIR-VIS ($w_{NIR}$=0.5, $w_{VIS}$=0.5) |
|---|---|---|---|---|---|---|
| EER (%) | 3.97 | 6.56 | 3.05 | 2.86 | 3.10 | 3.02 |
| Recognition (%) at 0.1 FAR | 97.82 | 94.79 | 98.55 | 98.60 | 98.42 | 98.55 |

## IX. ACKNOWLEDGEMENTS

We would like to thank University of Notre Dame (UND) and IIIT Delhi for providing us the databases.

## APPENDIX A
## CROSS-SENSOR IRIS RECOGNITION USING IRISCODES

Authors in [13] proposed a promising framework to improve the matching performance for cross-sensor adaptation in two different phases using conventional iris codes. In the first phase, few training samples are selected from two different iris readers. These samples are used to learn the adaptation parameters from optimized kernel matrix using the initial kernel matrix calculated with similarity measures of all selected samples. A convex optimization problem is formulated to minimize the logDet divergence [45] between the initial kernel matrix and adapted kernel matrix. The sensor adaptation parameters are calculated by imposing the distance preserving constraints [46] and application-specific constraints. The distance constraints are chosen as $20^{th}$ percentile of similar class distances and $85^{th}$ percentile of dissimilar class distances. In the second phase, these parameters are incorporated while iris matching in transformed domain. The performance of cross-sensor iris recognition is summarized in Table XI for the UND dataset.

It can be observed from the results presented in Table XI, the matching accuracy has been improved by 3.48% (in the entire dataset) whereas it was only 1.6% improvement (in properly segmented iris images from subset data).The algorithm is expected to perform better with well-segmented iris images rather than data with error in iris segmentation. The results reported in [13] can not be reproduced, because of some ambiguity in Section 6.3 (Equation 20), when we perform verification between a test sample ($\theta_t$) with enrolled sample.

TABLE XI
PERFORMANCE DEGRADATION FOR CROSS-SENSOR IRIS MATCHING: EER AND VERIFICATION RATE ON UND DATASET

| Comparisons | EER (%) (Entire dataset) | TAR (%) at FRR=0.1 (Entire dataset) | TAR (%) at FRR=0.1 (UND Subset) |
|---|---|---|---|
| LG2200 | 6.06 | 86.74 | 93.53 |
| LG4000 | 5.22 | 91.39 | 97.61 |
| Cross-sensor | 7.19 | 84.34 | 91.93 |
| Adapted | 6.09 | 87.82 | 93.78 |

It is mentioned that the squared Euclidean distance in the transformed domain is computed based on the training samples $\forall\theta$. One more ambiguity in this paper is that the sensor specific constraints are not included in the final optimization problem. We tried to reproduce the results with the assumptions that the Equation 20 (in section 6.3) means the verification should perform between a test sample with all enrolled samples. However these results were quite poor even after applying adaptation using kernel transformation learning.

## REFERENCES

[1] J. G. Daugman, "High confidence visual recognition of persons by a test of statistical independence," *IEEE Trans. Pattern Analysis and Machine Intelligence*, vol. 15, no. 11, pp. 1148–1161, 1993.
[2] M. J. Burge and K. Bowyer, *Handbook of Iris Recognition*. Science & Business Media, Springer, 2013.
[3] K. W. Bowyer, K. Hollingsworth, and P. J. Flynn, "Image understanding for iris biometrics: A survey," *Computer vision and image understanding*, vol. 110, no. 2, pp. 281–307, 2008.
[4] C.-W. Tan and A. Kumar, "Towards online iris and periocular recognition under relaxed imaging constraints," *IEEE Trans. Image Processing*, vol. 22, no. 10, pp. 3751–3765, 2013.
[5] Z. Zhao and A. Kumar, "An accurate iris segmentation framework under relaxed imaging constraints using total variation model," *Proc. ICCV 2015*, pp. 3828–3836, Santiago, Dec. 2015.

[6] S. T. Q. C. Directorate, "Bio-metric devices testing and certification," http://www.stqc.gov.in/content/about-certification/.

[7] O. Boiman, E. Shechtman, and M. Irani, "In defense of nearest-neighbor based image classification," *Proc. CVPR 2008*, pp. 1–8, 2008.

[8] Z. Wang, Y. Hu, and L.-T. Chia, "Image-to-class distance metric learning for image classification," *Proc. ECCV 2010*, pp. 706–719, 2010.

[9] R. Behmo, P. Marcombes, A. Dalalyan, and V. Prinet, "Towards optimal naive bayes nearest neighbor," *Proc. ECCV 2010*, pp. 171–184, 2010.

[10] T. Tommasi and B. Caputo, "Frustratingly easy nbnn domain adaptation," *Proc. ICCV 2013*, pp. 897–904, 2013.

[11] S. Lazebnik, C. Schmid, and J. Ponce, "Beyond bags of features: Spatial pyramid matching for recognizing natural scene categories," *Proc. CVPR 2006*, vol. 2, pp. 2169–2178, 2006.

[12] N. P. Ramaiah and A. Kumar, "Towards more accurate iris recognition using bi-spectral imaging and cross-spectral matching capability," *Technical Report No. COMP-K-21*, Dec. 2015.

[13] J. K. Pillai, M. Puertas, and R. Chellappa, "Cross-sensor iris recognition through kernel learning," *IEEE Trans. Pattern Analysis and Machine Intelligence*, vol. 36, no. 1, pp. 73–85, 2014.

[14] *The Hong Kong Polytechnic University Cross-Spectral Iris Image Database*, 2015, http://www.comp.polyu.edu.hk/˜csajaykr/polyuiris.htm.

[15] J. Zuo, F. Nicolo, N. Schmid *et al.*, "Cross spectral iris matching based on predictive image mapping," in *Proc. IEEE Int.l Conf. Biometrics: Theory Applications and Systems (BTAS)*, 2010, pp. 1–5.

[16] L. Xiao, Z. Sun, R. He, and T. Tan, "Coupled feature selection for cross-sensor iris recognition," in *Proc. IEEE Int.l Conf. Biometrics: Theory, Applications and Systems (BTAS)*, 2013, pp. 1–6.

[17] C.-W. Tan and A. Kumar, "Unified framework for automated iris segmentation using distantly acquired face images," *IEEE Trans. Image Processing*, vol. 21, no. 9, pp. 4068–4079, 2012.

[18] A. Ross, R. Pasula, and L. Hornak, "Exploring multispectral iris recognition beyond 900nm," in *Proc. IEEE Int.l Conf. Biometrics: Theory, Applications, and Systems*, 2009, pp. 1–8.

[19] A. Sharma, S. Verma, M. Vatsa, and R. Singh, "On cross spectral periocular recognition," in *Proc. IEEE Int.l Conf. Image Processing (ICIP)*, 2014, pp. 5007–5011.

[20] K. W. Bowyer, S. E. Baker, A. Hentz, K. Hollingsworth, T. Peters, and P. J. Flynn, "Factors that degrade the match distribution in iris biometrics," *Identity in the Information Society*, vol. 2, no. 3, pp. 327–343, 2009.

[21] R. Connaughton, A. Sgroi, K. W. Bowyer, and P. Flynn, "A cross-sensor evaluation of three commercial iris cameras for iris biometrics," in *Proc. IEEE Computer Society Conf. Computer Vision and Pattern Recognition Workshops (CVPRW)*, 2011, pp. 90–97.

[22] R. Connaughton, A. Sgroi, K. Bowyer, and P. J. Flynn, "A multialgorithm analysis of three iris biometric sensors," *IEEE Trans. Information Forensics and Security*, vol. 7, no. 3, pp. 919–931, 2012.

[23] S. S. Arora, M. Vatsa, R. Singh, and A. Jain, "On iris camera interoperability," in *Proc. IEEE Int.l Conf. Biometrics: Theory, Applications and Systems (BTAS)*, 2012, pp. 346–352.

[24] R. Jillela and A. Ross, "Matching face against iris images using periocular information," in *2014 IEEE International Conference on Image Processing (ICIP)*. IEEE, 2014, pp. 4997–5001.

[25] G. Santos, E. Grancho, M. V. Bernardo, and P. T. Fiadeiro, "Fusing iris and periocular information for cross-sensor recognition," *Pattern Recognition Letters*, vol. 57, pp. 52–59, 2015.

[26] R. Gopalan, R. Li, and R. Chellappa, "Domain adaptation for object recognition: An unsupervised approach," *Proc. ICCV 2011*, pp. 999–1006, 2011.

[27] K. Saenko, B. Kulis, M. Fritz, and T. Darrell, "Adapting visual category models to new domains," *Proc. ECCV 2010*, pp. 213–226, 2010.

[28] R. Gopalan, R. Li, and R. Chellappa, "Unsupervised adaptation across domain shifts by generating intermediate data representations," *IEEE transactions on pattern analysis and machine intelligence*, vol. 36, no. 11, pp. 2288–2302, 2014.

[29] B. Gong, Y. Shi, F. Sha, and K. Grauman, "Geodesic flow kernel for unsupervised domain adaptation," *Proc. CVPR 2012*, pp. 2066–2073, 2012.

[30] B. Gong, K. Grauman, and F. Sha, "Learning kernels for unsupervised domain adaptation with applications to visual object recognition," *International Journal of Computer Vision*, vol. 109, no. 1-2, pp. 3–27, 2014.

[31] L. Duan, I. W. Tsang, D. Xu, and S. J. Maybank, "Domain transfer svm for video concept detection," *Proc. CVPR 2009*, pp. 1375–1381, 2009.

[32] A. Khosla, T. Zhou, T. Malisiewicz, A. A. Efros, and A. Torralba, "Undoing the damage of dataset bias," *Proc. ECCV 2012*, pp. 158–171, 2012.

[33] L. Masek and P. Kovesi, *Matlab source code for a biometric identification system based on iris patterns*, 2003, http://www.csse.uwa.edu.au/˜pk/studentprojects/libor/index.html.

[34] W. T. Freeman, E. C. Pasztor, and O. T. Carmichael, "Learning low-level vision," *International journal of computer vision (IJCV)*, vol. 40, no. 1, pp. 25–47, 2000.

[35] X. Wang and X. Tang, "Face photo-sketch synthesis and recognition," *IEEE Trans. Pattern Analysis and Machine Intelligence*, vol. 31, no. 11, pp. 1955–1967, 2009.

[36] J. S. Yedidia, W. T. Freeman, and Y. Weiss, "Understanding belief propagation and its generalizations," *Exploring Artificial Intelligence in the new millennium*, vol. 8, pp. 236–239, 2003.

[37] H. Proença and L. A. Alexandre, "Ubiris: A noisy iris image database," in *Image Analysis and Processing*, 2005, pp. 970–977.

[38] H. Proenca, S. Filipe, R. Santos, J. Oliveira, L. Alexandre *et al.*, "The ubiris. v2: A database of visible wavelength iris images captured on-the-move and at-a-distance," *IEEE Trans. Pattern Analysis and Machine Intelligence*, vol. 32, no. 8, pp. 1529–1535, 2010.

[39] D. Yadav, N. Kohli, J. S. Doyle, R. Singh, M. Vatsa, and K. W. Bowyer, "Unraveling the effect of textured contact lenses on iris recognition," *IEEE Trans. Information Forensics and Security*, vol. 9, no. 5, pp. 851–862, 2014.

[40] N. Kohli, D. Yadav, M. Vatsa, and R. Singh, "Revisiting iris recognition with color cosmetic contact lenses," in *Proc. Int.l Conf. Biometrics (ICB)*, 2013, pp. 1–7.

[41] Y. Lee, R. Micheals, J. Filliben, and P. Phillips, "Robust iris recognition baseline for the grand challenge," *NIST-IR report*, vol. 7777, 2011.

[42] L. Ma, T. Tan, Y. Wang, and D. Zhang, "Personal identification based on iris texture analysis," *IEEE Trans. Pattern Analysis and Machine Intelligence*, vol. 25, no. 12, pp. 1519–1533, 2003.

[43] J. Gan and Y. Liang, "Applications of wavelet packets decomposition in iris recognition," in *Advances in Biometrics*, 2005, pp. 443–449.

[44] *Weblink for downloading codes for all algorithms in this paper*, 2016, http://www.comp.polyu.edu.hk/˜csajaykr/cross-iris.htm.

[45] B. Kulis, M. Sustik, and I. Dhillon, "Learning low-rank kernel matrices," in *Proc. ACM Int.l Conf. Machine learning*, 2006, pp. 505–512.

[46] J. V. Davis, B. Kulis, P. Jain, S. Sra, and I. S. Dhillon, "Information-theoretic metric learning," in *Proc. ACM Int.l Conf. Machine learning*, 2007, pp. 209–216.